J|A|C|S
ARTICLES
Published on Web 09/14/2006

Self-Assembly of Small Gold Nanoparticles through Interligand Interaction

Masayuki Kanehara, Etsushi Kodzuka, and Toshiharu Teranishi*

Contribution from the Graduate School of Pure and Applied Sciences, University of Tsukuba, 1-1-1 Tennodai, Tsukuba, Ibaraki 305-8571, Japan

Received June 26, 2006; E-mail: teranisi@chem.tsukuba.ac.jp

Abstract: Stable and monodisperse Au nanoparticles smaller than 2 nm are easily prepared by the reduction of $HAuCl_4 \cdot 4H_2O$ in DMF/H_2O in the presence of a series of bidentate ligands, 2,6-bis(1′-(*n*-thioalkyl)-benzimidazol-2-yl)pyridine (TC_nBIP, $n = 3$, 6, 8, 10, 12). The TC_nBIP ligands afford stronger coordination ability than alkanethiols due to their bidentate nature. These small nanoparticles form hexagonal close-packed (hcp) two-dimensional (2D) superlattices with tunable interparticle spacings (from 1.2 to 2.5 nm), produced by changing the length of the ligand at both the hydrophobic amorphous carbon and the air−water interface. Long-range-ordered hcp 2D superlattices were fabricated through the cleavage and construction of interligand $\pi-\pi$ interactions formed via an annealing process at the air−water interface.

Introduction

Chemical techniques for the preparation and size separation of organically protected metal and semiconductor nanoparticles have advanced rapidly over the past several years.[1−10] From the discovery of a Coulomb staircase through the double-tunnel junction,[11] metal nanoparticles have also attracted much attention for their potential in single-electron-tunneling devices.[12] Recent synthetic developments in the fabrication of highly monodisperse metal nanoparticles allow us to study not only the properties of the individual nanoparticles, but also the collective effects of the two-dimensional (2D) and three-dimensional (3D) superlattices of metal nanoparticles on their physical properties.[13−23] The in-plane electron transport characteristics of metal nanoparticle 2D superlattices are strongly affected by the following three types of disorder: global structural disorder in the array topology, local structural disorder in the interparticle couplings, and local charge disorder, due to random immobile charges in the underlying substrate.[16] To minimize an unpredictable disorder effect, the fabrication of well-ordered metal nanoparticle 2D superlattices is of great importance. For the development of practical nanoelectronic devices based on the single-electron-tunneling effect at room temperature, it is indispensable to reveal the electron transport properties of well-ordered 2D superlattices of small (<2 nm) nanoparticles, which are expected to show the Coulomb-blockade phenomenon at room temperature. Although the fabrication techniques of relatively large metal and semiconductor nanoparticle superlattices have been vigorously investigated so far, well-ordered superlattices made from quite small (<2 nm) particles are still limited. Whetten et al. reported self-assembled, well-ordered hexagonal close-packed (hcp) 2D superlattices of water-soluble *Greengold*, where the 1.3 nm Au cores are protected by amide-terminated PR_3 compounds ($R = p\text{-}C_6H_4CONHCH_3$).[24] An alternative technique for the fabrication of ordered monolayers of Au cluster compounds has been reported by Schmid's group.[25] Here, the authors utilized the strong attractive interactions between

(1) Brust, M.; Walker, M.; Bethell, D.; Schiffrin, D. J.; Whyman, R. *Chem. Commun.* **1994**, 801−802.
(2) Teranishi, T.; Kiyokawa, I.; Miyake, M. *Adv. Mater.* **1998**, *10*, 596−599.
(3) Teranishi, T.; Hasegawa, S.; Shimizu, T.; Miyake, M. *Adv. Mater.* **2001**, *13*, 1699−1701.
(4) Shimizu, T.; Teranishi, T.; Hasegawa, S.; Miyake, M. *J. Phys. Chem. B* **2003**, *107*, 2719−2724.
(5) Li, L.; Walda, J.; Manna, L.; Alivisatos, A. P. *Nano Lett.* **2002**, *2*, 557−560.
(6) Puntes, V. F.; Krishnan, K. M.; Alivisatos, P. *Science* **2001**, *291*, 2115−2117.
(7) Murray, C. B.; Norris, D. J.; Bawendi, M. G. *J. Am. Chem. Soc.* **1993**, *115*, 8706−8715.
(8) Sun, Y.; Xia, Y. *Science* **2002**, *298*, 2176−2179.
(9) Sun, S.; Murray, C. B.; Weller, D.; Folks, L.; Moser, A. *Science* **2000**, *287*, 1989−1992.
(10) Jin, R.; Cao, Y. C.; Hao, E.; Metraux, G. S.; Schatz, G. C.; Mirkin, C. A. *Nature* **2003**, *425*, 487−490.
(11) Andres, R. P.; Bein, T.; Dorogi, M.; Feng, S.; Henderson, J. I.; Kubiak, C. P.; Mahoney, W.; Osifchin, R. G.; Reifenberger, R. *Science* **1996**, *272*, 1323−1325.
(12) Azuma, Y.; Kanehara, M.; Teranishi, T.; Majima, Y. *Phys. Rev. Lett.* **2006**, *98*, 016108(1−4).
(13) Kanehara, M.; Oumi, Y.; Sano, T.; Teranishi, T. *J. Am. Chem. Soc.* **2003**, *125*, 8708−8709.
(14) Sohn, B.-H.; Choi, J.-M.; Yoo, S. I.; Yun, S.-H.; Zin, W.-C.; Jung, J. C.; Kanehara, M.; Hirata, T.; Teranishi, T. *J. Am. Chem. Soc.* **2003**, *125*, 6368−6369.
(15) Teranishi, T.; Sugawara, A.; Shimizu, T.; Miyake, M. *J. Am. Chem. Soc.* **2002**, *124*, 4210−4211.
(16) Parthasarathy, R.; Lin, X.-M.; Jaeger, H. M. *Phys. Rev. Lett.* **2001**, *87*, 186807(1−4).
(17) Shiang, J. J.; Heath, J. R.; Collier, C. P.; Saykally, R. J. *J. Phys. Chem. B* **1998**, *102*, 3425−3430.
(18) Kim, S.-H.; Medeiros-Ribeiro, G.; Ohlberg, D. A. A.; Williams, R. S.; Heath, J. R. *J. Phys. Chem. B* **1999**, *103*, 10341−10347.
(19) Sampaio, J. F.; Beverly, K. C.; Heath, J. R. *J. Phys. Chem. B* **2001**, *105*, 8797−8800.
(20) Beverly, K. C.; Sampaio, J. F.; Heath, J. R. *J. Phys. Chem. B* **2002**, *106*, 2131−2135.
(21) Collier, C. P.; Saykally, R. J.; Shiang, J. J.; Henrichs, S. E.; Heath, J. R. *Science* **1997**, *277*, 1978−1981.
(22) Redl, F. X.; Cho, K.-S.; Murray, C. B.; O'brien, S. *Nature* **2003**, *423*, 968−971.
(23) Shevchenko, E. V.; Talapin, D. V.; O'Brien, S.; Murray, C. B. *J. Am. Chem. Soc.* **2005**, *127*, 8741−8747.
(24) Gutierrez, E.; Powell, R. D.; Furuya, F. R.; Hainfeld, J. F.; Schaaff, T. G.; Shafigullin, M. N.; Stephens, P. W.; Whetten, R. L. *Eur. Phys. J. D* **1999**, *9*, 647−651.

10.1021/ja064510q CCC: $33.50

polyelectrolytes, in which the imino groups on a substrate and sulfonic groups on the cluster surfaces were used to promote the self-assembly of the acidic $[Au_{55}\{PPh_2(m\text{-}C_6H_4SO_3Na)_{12}\}Cl_6]$ on a mica surface coated with poly(ethylenimine). In both cases, however, the phosphine-capped nanoparticles are so unstable that it is difficult to measure the physical properties of the superlattices.

In addition to these disorder effects, the control of the interparticle spacings, and the chemical structure of the ligands greatly affecting the tunneling resistance, are key determinants of the electronic property of metal nanoparticle superlattices.[21,26−29] As for the interparticle spacing, we have recently demonstrated that, for ∼2 nm alkanethiol-protected Au nanoparticles, the tunneling resistance of the alkanethiol layer changes from 8.5 GΩ (1-octanethiol) to 500 MΩ (1-hexanethiol), implying that the shorter ligand is desirable for a drastic reduction of the tunneling resistance. Furthermore, the introduction of a π-conjugated unit to the ligand would also reduce the tunneling resistance. On the other hand, it has been proposed that the electrical properties of organic molecules can be controlled by the occupancy of energy levels within these molecules, as illustrated by the use of oligophenylene−ethynylene[30] and viologen bridges.[31] In both cases, it was found that charge trapping in molecular states leads to changes in electrical behavior. Well-ordered metal nanoparticle superlattices having redox-active organic units between the particles have a great potential for numerous device applications, including high-frequency oscillators, mixers, multipliers, analog-to-digital converters, etc.[31] Benzimidazoles and substituted benzimidazoles show excellent electron-conductive properties, and have been used as redox-active sites in electron-conductive polymers.[32] We previously reported the preparation of 1.9 nm monodisperse Au nanoparticles protected by the benzimidazole derivative 2,6-bis(1′-(8-thiooctyl)benzimidazol-2-yl)pyridine (TC_8BIP). These protected nanoparticles have quite narrow size distribution and have been shown to remain stably dispersed in DMF for more than one year.[33] Well-ordered 2D superlattices of these Au nanoparticles were obtained through the self-assembly process on an amorphous-carbon-coated copper grid, probably due to $\pi-\pi$ interactions between the neighboring 2,6-bis(benzimidazol-2-yl)pyridine (BIP) groups of the TC_8BIP layers.

To reveal the electron-transport properties of 2D superlattices of redox-active organic unit surrounded small nanoparticles, establishing a general fabrication technique of a well-ordered small metal nanoparticle superlattice is indispensable. In this paper, we report the fabrication of hcp 2D superlattices of small (1.5−2.2 nm) Au nanoparticles, whose protective ligands are terminated with redox-active π-conjugated aromatic groups. After synthesis of a series of 2,6-bis(1′-(*n*-thioalkyl)benzimidazol-2-yl)pyridines (TC_nBIPs, $n = 3, 5, 8, 10, 12$), TC_nBIP-protected small Au nanoparticles were self-assembled into well-ordered hcp 2D superlattices, both on an amorphous-carbon-coated Cu grid and on an air−water interface, where the interparticle spacings were tuned according to the length of the TC_nBIP ligands. Well-ordered hcp superlattices of TC_nBIP-protected Au nanoparticles on water were subject to an annealing process to achieve the long-range ordering of small Au nanoparticles.

Results and Discussion

General Remarks on Ligand Syntheses. To demonstrate our concept for the formation of well-ordered hcp 2D superlattices of small nanoparticles based on the interligand $\pi-\pi$ interactions, we focused on the syntheses of a series of TC_n-BIP ligands ($n = 3, 6, 8, 10, 12$). These ligands were designed to have three functional groups, that is, disulfide groups to coordinate with the surface Au atoms of the nanoparticles, BIP groups to promote interligand $\pi-\pi$ interactions and endow redox-active sites to particles, and alkyl chains to control interparticle spacings.

A previously reported synthetic route to TC_8BIP ligands involved the substitution of dibromoalkane with BIP in the first step.[33] This procedure principally affords unsatisfactory yields of bissubstituted bromoalkyl-BIP due to an intramolecular ring formation. To avoid this reaction, bromoalkene was used instead of dibromoalkane. Scheme 1 shows the new synthetic routes for a series of TC_nBIP molecules. In the synthesis of $TC_{10}BIP$, the olefin **1** was synthesized through the mild bromination of 9-decen-1-ol with triphenylphosphine and tetrabromomethane. The substitution of bromoalkenes with BIP gives the terminal olefins **2a**−**d** in satisfactory yields. The terminal olefin reacts with thioacetic acid under UV irradiation to give the anti-Markovnikov product. These reactions afford almost equivalent yields of the terminal thioacetoxy derivatives **3a**−**d** without any radical initiators. For the synthesis of terminal bromododecyl-BIP **2e**, 10 equiv of 1,12-dibromododecane was used in quite high concentration (dibromododecane:solvent = 1:1 (v/v)) to prevent an undesirable intramolecular ring formation, the yield of **2e** being 75%. The thioacetate **3e** was equivalently obtained from **2e** and potassium thioacetate. The reduction of **3a** using $NaBH_4$ gives the reduced form of TC_3BIP in excellent yield (93%), while alcoholysis and mild oxidation of **3b**−**e** afford the final products **4b**−**e** in satisfactory yields (71−93%).

Formation of TC_nBIP−Au Nanoparticles. The TC_nBIP-protected Au (TC_nBIP−Au) nanoparticles were synthesized by the $NaBH_4$ reduction of $HAuCl_4{\cdot}4H_2O$ in the presence of a series of TC_nBIP ligands in a DMF/H_2O mixed solution. The solution turned from yellow to brown-red immediately after the addition of $NaBH_4$ aqueous solution. Figure 1 shows the representative UV−vis spectra of the solutions containing $HAuCl_4{\cdot}4H_2O$ and TC_3BIP, TC_8BIP, or $TC_{12}BIP$ (TC_nBIP:Au = 1:1 (mol/mol)) before and after addition of $NaBH_4$ aqueous solution. In the UV−vis spectra of the resulting solutions, the peak at 320 nm assigned to the charge-transfer transition of $[AuCl_4]^-$ ions and the $\pi-\pi^*$ transition of TC_nBIP (BIP groups) decreased after addition of $NaBH_4$, and broad tailing absorptions were observed between the ultraviolet and visible regions due to development of the band structure, indicating the formation

(25) Schmid, G.; Baumle, M.; Beyer, N. *Angew. Chem., Int. Ed.* **2000**, *39*, 181−183.
(26) Maye, M. M.; Chun, S. C.; Han, L.; Rabinovich, D.; Zhong, C.-J. *J. Am. Chem. Soc.* **2002**, *124*, 4958−4959.
(27) Maye, M. M.; Luo, J.; Lim, I.-I. S.; Han, L.; Kariuki, N. N.; Rabinovich, D.; Liu, T.; Zhong, C.-J. *J. Am. Chem. Soc.* **2003**, *125*, 9906−9907.
(28) Frankamp, B. L.; Boal, A. K.; Rotello, V. M. *J. Am. Chem. Soc.* **2002**, *124*, 15146−15147.
(29) Black, C. T.; Murray, C. B.; Sandstrom, R. L.; Sun, S. *Science* **2000**, *290*, 1131−1134.
(30) Chen, J.; Reed, M. A.; Rawlett, A. M.; Tour, J. M. *Science* **1999**, *286*, 1550−1552.
(31) Gittins, D. I.; Bethell, D.; Schiffrin, D. J.; Nichols, R. J. *Nature* **2000**, *408*, 67−69.
(32) Yu, S. C.; Hou, S.; Chan, W. K. *Macromolecules* **1999**, *32*, 5251−5256.
(33) Teranishi, T.; Haga, M.; Shiozawa, Y.; Miyake, M. *J. Am. Chem. Soc.* **2000**, *122*, 4237−4238.

Scheme 1. Synthetic Procedures of TC_nBIP Ligands

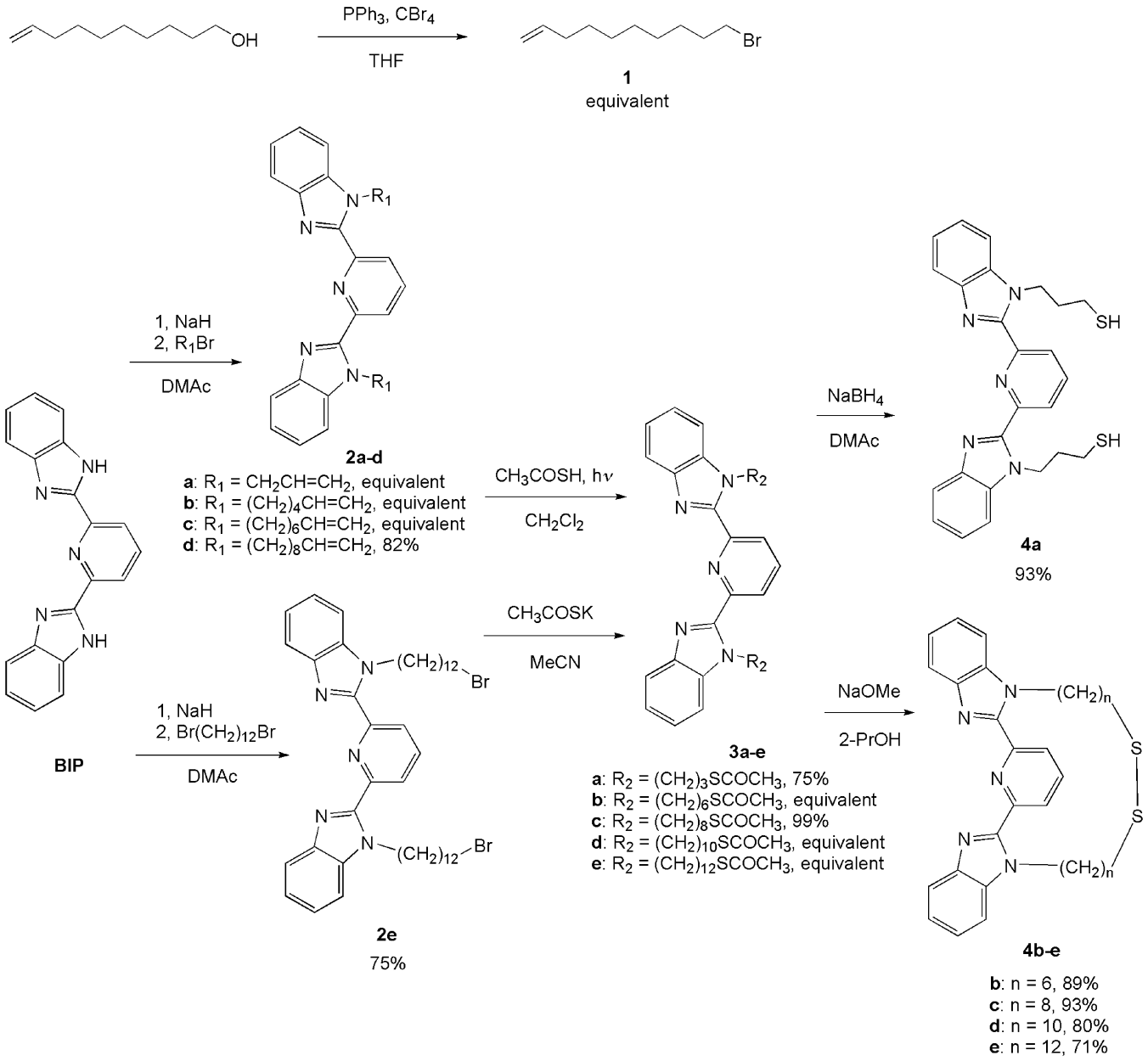

of Au nanoparticles. Small surface plasmon resonance bands around 520 nm were observed for all samples, indicating that a small amount of larger nanoparticles is contained in the solution. The other $TC_nBIP-Au$ nanoparticles showed similar spectra depending on their sizes. These Au nanoparticles have been shown to remain stably dispersed in a DMF/H_2O mixed solution under air for at least one year, probably due to their bidentate nature.

Table 1 presents the mean diameters and standard deviations of Au nanoparticles prepared at various TC_nBIP:Au molar ratios. Both the mean diameter and standard deviation decreased with an increase in the amount of the protective agent, TC_nBIP, which was also observed in the cases involving polymer-protected Pd,[34] Pt,[35,36] and Au[2] nanoparticles. For TC_nBIP ($n = 8, 10, 12$), Au nanoparticles smaller than 2 nm could be obtained for TC_nBIP:Au molar ratios larger than 1.0. For $TC_6BIP-Au$, 1.8 nm particles were obtained when the TC_6BIP:Au molar ratio was 2.0. On the other hand, when using TC_3BIP as a protective ligand, only Au nanoparticles larger than 2 nm were produced even at large TC_3BIP:Au molar ratios. Generally, to prepare kinetically stabilized small Au nanoparticles, sterically bulky ligands[37−40] and a low reaction temperature[41] have been employed, because the growth rate of the metal core may decrease with increasing ligand bulkiness and decreasing reaction temperature. Our $TC_nBIP-Au$ nanoparticles follow this

(34) Teranishi, T.; Miyake, M. *Chem. Mater.* **1998**, *10*, 594−600.
(35) Teranishi, T.; Hosoe, M.; Tanaka, T.; Miyake, M. *J. Phys. Chem. B* **1999**, *103*, 3818−3827.
(36) Teranishi, T.; Hosoe, M.; Miyake, M. *Adv. Mater.* **1997**, *9*, 65−67.
(37) Wuelfing, W. P.; Gross, S. M.; Miles, D. T.; Murray, R. W. *J. Am. Chem. Soc.* **1998**, *120*, 12696−12697.
(38) Templeton, A. C.; Chen, S.; Gross, S. M.; Murray, R. W. *Langmuir* **1999**, *15*, 66−76.
(39) Brown, L. O.; Hutchison, J. E. *J. Am. Chem. Soc.* **1999**, *121*, 882−883.
(40) Daniel, M.-C.; Astruc, D. *Chem. Rev.* **2004**, *104*, 293−346.
(41) Negishi, Y.; Takasugi, Y.; Sato, S.; Yao, H.; Kimura, K.; Tsukuda, T. *J. Am. Chem. Soc.* **2004**, *126*, 6518−6519.

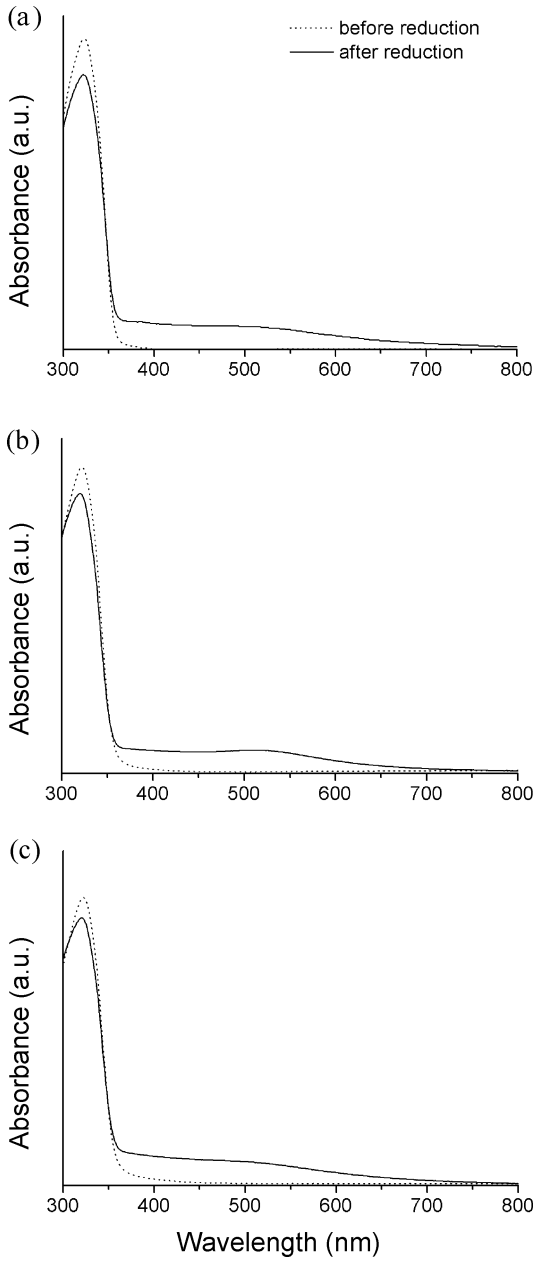

Figure 1. UV−vis spectra of the solutions containing $HAuCl_4 \cdot 4H_2O$ before and after addition of a $NaBH_4$ aqueous solution in the presence of (a) TC_3-BIP, (b) TC_8BIP, and (c) TC_{12}BIP.

tendency; that is, TC_nBIP ligands with a longer alkyl chain tend to produce smaller Au nanoparticles at a similar TC_nBIP:Au ratio. In addition, it is well-known that small gold clusters exhibit a strong fluorescence; however, the TC_nBIP−Au nanoparticles described here are larger than the fluorescent gold clusters and do not exhibit fluorescence.

Characterization of TC_nBIP−Au Nanoparticles. High-resolution transmission electron microscopy (HRTEM) provides extensive information about the size and crystal structure of inorganic nanoparticles. As shown in Figure 2, an HRTEM image of 1.5 nm TC_{12}BIP−Au shows lattice fringes originating from a single crystal, and the lattice spacing of 0.24 nm is in good agreement with that of the (111) plane (0.2355 nm) for fcc bulk Au. The crystal structure of the TC_nBIP−Au nanoparticles was also confirmed by X-ray diffraction (XRD) measurements. An XRD pattern of the 1.9 nm TC_8BIP−Au

Table 1. Mean Diameters and Standard Deviations of a Series of TC_nBIP−Au Nanoparticles Synthesized at Various TC_nBIP:Au Molar Ratios

ligand	TC_nBIP:Au (mol/mol)	mean diam (nm)	std dev (nm)
TC_3BIP	1.0	2.7	1.0
	2.0	2.2	0.5
TC_6BIP	1.0	2.6	0.9
	2.0	1.6	0.5
TC_8BIP	0.05	3.2	0.8
	0.1	2.7	0.5
	0.5	2.3	0.4
	1.0	1.9	0.4
	2.0	1.5	0.2
TC_{10}BIP	1.0	1.6	0.3
	2.0	1.5	0.2
TC_{12}BIP	0.4	1.6	0.5
	0.5	1.6	0.4
	1.0	1.5	0.3
	2.0	1.5	0.3

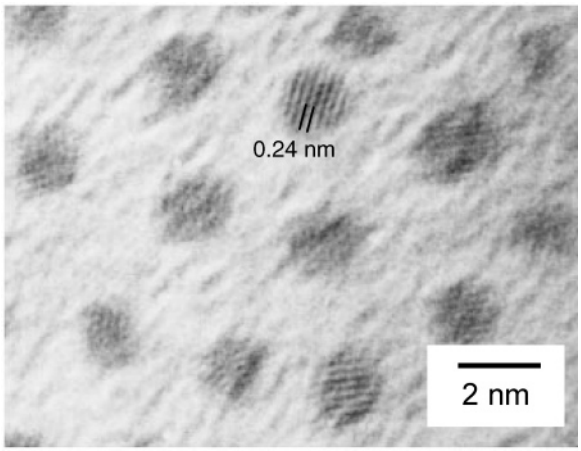

Figure 2. High-resolution TEM image of 1.5 nm TC_8BIP−Au nanoparticles.

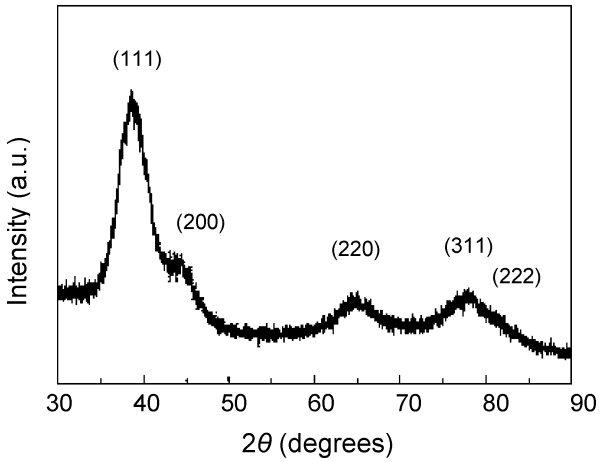

Figure 3. XRD pattern of 1.9 nm TC_8BIP−Au nanoparticles.

nanoparticles is representatively shown in Figure 3. Several diffraction peaks were observed at 38.1°, 44.4°, 64.8°, 77.8°, and 82.2°, which correspond to the (111), (200), (220), (311), and (222) planes of the fcc bulk Au, respectively. Other TC_n-BIP−Au nanoparticles also show similar XRD patterns with slight differences in the fwhm values. The chemical state of gold in the TC_nBIP−Au nanoparticles was confirmed by X-ray photoelectron spectroscopy (XPS). The $Au4f_{7/2}$ binding energies

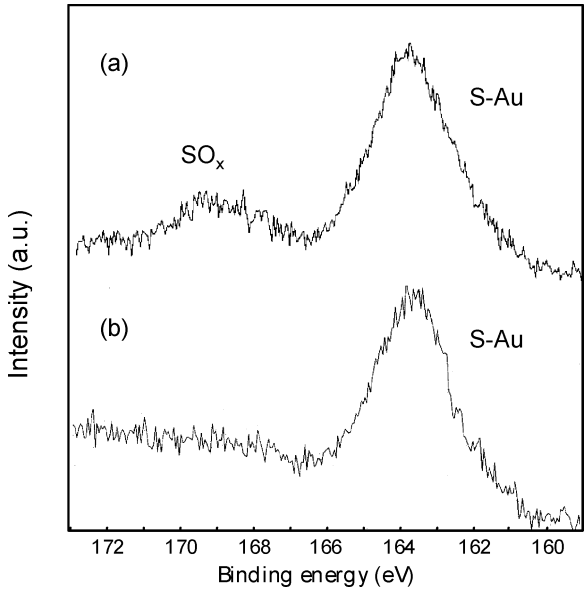

Figure 4. S2p XPS spectra of (a) as-synthesized and (b) purified TC_8BIP−Au nanoparticles.

of TC_nBIP−Au nanoparticles have peaks centered at 84.0 eV. The Au substrate covered with a 2D self-assembled monolayer of alkanethiol (where the alkanethiol coverage is 33%) showed a $Au4f_{7/2}$ binding energy (84.0 ± 0.1 eV) similar to that of bulk Au (84.0 eV).[42] On dodecanethiol-protected Au nanoparticles (diameter 2.0−2.5 nm, ∼60% coverage based on a ∼309 atom core), Brust et al. observed a similar $Au4f_{7/2}$ peak value.[1] It was thus a question of whether smaller cluster cores would continue to exhibit bulk metal-like photoionization.

Then, the TC_nBIP ligands protecting Au nanoparticles were characterized by XPS, Fourier transform infrared (FT-IR) measurements, and thermogravimetric analysis (TGA). Figure 4 shows the high-resolution S2p core level XPS spectra of as-synthesized and purified 1.9 nm TC_8BIP−Au nanoparticles. After purification, the S2p peak at 169 eV assigned to sulfur oxide (SO_x) disappeared without a significant decrease in the S2p peak at 163.5 eV assigned to thiolates, meaning that the pure Au nanoparticles were obtained by the repeated-precipitation technique, which is indispensable for the formation of a long-range-ordered 2D superlattice of nanoparticles. The S2p binding energy for TC_8BIP−Au (163.5 eV) is comparable to that of alkanethiol-protected Au nanoparticles,[43] indicating that the thiolate coordination site of the TC_8BIP ligand possesses a binding ability similar to that of alkanethiol.

FT-IR spectroscopy was adopted to investigate the conformation of alkyl chains of TC_nBIP ligands on the surface of Au nanoparticles. The peak positions for the symmetric (d^+) and asymmetric (d^-) stretching bands of the methylene C−H bonds can be used as a sensitive indicator to estimate the degree of ordering of alkyl chains.[4] For crystalline polyethylene (all-trans zigzag confirmation), the d^+ and d^- bands appear at 2920 and 2850 cm^{-1}, respectively, and these shift to 2928 and 2856 cm^{-1} for amorphous polyethylene (coexistence of trans and gauche conformations), respectively. The methylene peaks corresponding to the d^+ and d^- bands appeared at 2920 and 2850 cm^{-1} for all TC_nBIP−Au, demonstrating that the alkyl chains of the TC_nBIP ligands on the Au surface predominantly have an all-trans conformation in the dry state.

Table 2. Au Contents and the Number of Surface Au Atoms Occupied by a Single Thiolate for TC_nBIP−Au Nanoparticles Synthesized at a Molar Ratio of TC_nBIP:Au = 1

ligand	mean diam (nm)	Au content[a] (wt %)	no. of surface Au atoms occupied by a single thiolate[b]
TC_8BIP	1.9	72.2	2.5
TC_{10}BIP	1.6	69.0	2.2
TC_{12}BIP	1.5	67.4	2.4

[a] Obtained from TGA measurement. [b] Calculated on the assumption that the particles have truncated octahedral shell structures.

The progressive heating of thiol-stabilized Au nanoparticles leads to volatilization of the organic fraction as disulfides, leaving a residue of gold.[44] Thus, TGA can provide information on the total organic content of the nanoparticles. Table 2 shows the representative Au contents of TC_nBIP−Au nanoparticles estimated by TGA, the Au contents of TC_8BIP−, TC_{10}BIP−, and TC_{12}BIP−Au being 72.2, 69.0, and 67.4 wt %, respectively. Table 2 also presents the number of surface Au atoms occupied by a single thiolate ligand, which was calculated on the assumption that the particle has a truncated octahedral shell structure, in which the bithiolate (two sulfur ends) of one TC_nBIP ligand protects a single Au nanoparticle. It was found that two or three surface Au atoms were occupied by a single thiolate group of the TC_nBIP ligand in all cases. These surface coverages are almost comparable to those of alkanethiol-protected Au nanoparticles.[43]

Self-Assembled 2D Monolayers of TC_nBIP−Au Nanoparticles. Figure 5 shows the TEM images of a self-assembled 2D monolayer of 2.2 nm TC_3BIP−, 1.8 nm TC_6BIP−, 1.9 nm TC_8BIP−, 1.6 nm TC_{10}BIP−, and 1.5 nm TC_{12}BIP−Au nanoparticles. Locally ordered hcp 2D domains were formed in all samples, among which the TC_nBIP−Au nanoparticles with relatively short chain lengths (n = 3, 6, 8) formed rather larger hcp domains. The ligand density around the Au core decreases with elongating alkyl chain length of the TC_nBIP ligand and may play an important role in the formation of well-ordered superlattices. To obtain well-ordered superlattices, an optimum outer density of effectively interactive aromatic BIP groups is needed. For 1.5 nm TC_8BIP−Au nanoparticles, the volume of the aromatic BIP groups is ca. 0.3 nm^3, considering that the π-orbital expansion centering on the BIP plane is 0.35 nm. Assuming the Au nanoparticles have a shell structure, the volume ratio of total BIP groups with respect to the BIP shell spread around the particle is ca. 20%. Since the well-ordered hcp 2D superlattices were obtained from TC_3BIP−, TC_6BIP−, and TC_8BIP−Au nanoparticles, an outer density of the effectively interactive BIP groups of >20% was needed in our samples. An introduction to the interactive aromatic groups of the ligand is feasible to form well-ordered hcp 2D superlattices of small nanoparticles. Since the BIP molecule has a highly crystallized nature and shows very low solubility in most organic solvents, the relatively strong interparticle interaction of TC_nBIP−Au nanoparticles may stabilize their 2D superlattices.

(42) Bain, C. D.; Biebuyck, H. A.; Whitesides, G. M. *Langmuir* **1989**, *5*, 723−727.
(43) Hostetler, M. J.; Wingate, J. E.; Zhong, C.-J.; Harris, J. E.; Vachet, R. W.; Clark, M. R.; Londono, J. D.; Green, S. J.; Stokes, J. J.; Wignall, G. D.; Glish, G. L.; Porter, M. D.; Evans, N. D.; Murray, R. W. *Langmuir* **1998**, *14*, 17−30.
(44) Gopidas, K. R.; Whitesell, J. K.; Fox, M. A. *J. Am. Chem. Soc.* **2003**, *125*, 6491−6502.

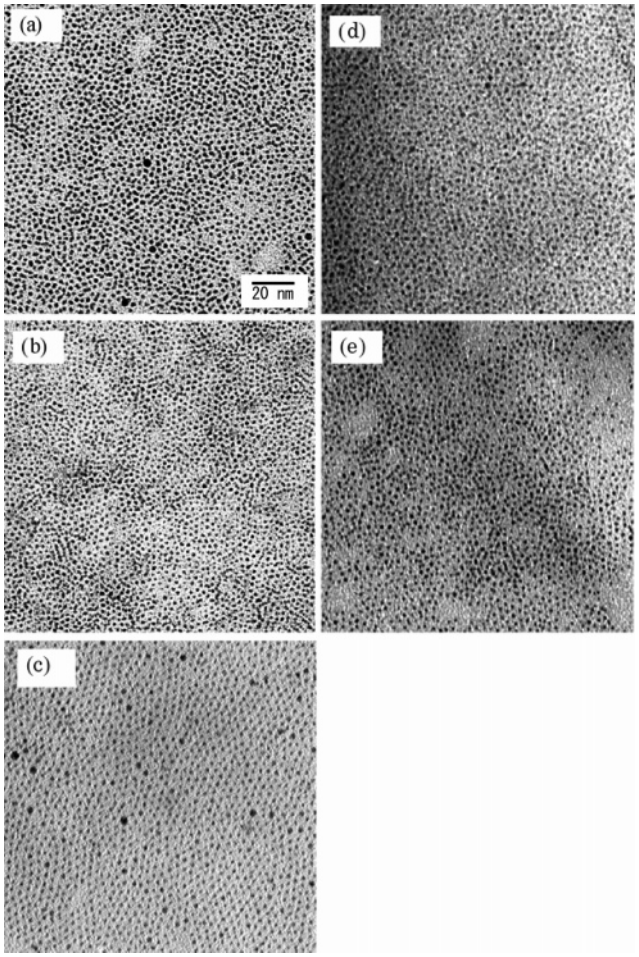

Figure 5. TEM images of a self-assembled 2D monolayer of (a) 2.2 nm TC_3BIP-, (b) 1.6 nm TC_6BIP-, (c) 1.9 nm TC_8BIP-, (d) 1.6 nm $TC_{10}BIP-$, and (e) 1.5 nm $TC_{12}BIP-$Au nanoparticles on carbon-coated Cu grids.

Heath et al. also reported the volume effect of linear alkyl ligand-protected Au and Ag nanoparticles in LB monolayers. The authors classified the nanoparticles into three categories depending on their outer ligand densities. The nanoparticles with an optimum ligand density gave well-ordered hcp 2D superlattices, while the nanoparticles with a low ligand density afforded only foamlike 2D structures.[45] It should be noted that the 2D superlattices of TC_nBIP-Au nanoparticles showed excellent stability against heat and electron beam irradiation during TEM observation due to a bidentate ligand structure, and as such, stability is quite important for measurements of both their physical properties and their applications.

The mean interparticle spacings from particle edge to edge for TC_3BIP-, TC_6BIP-, TC_8BIP-, $TC_{10}BIP-$, and $TC_{12}BIP-$Au superlattices were estimated from TEM images to be 1.2, 1.6, 1.9, 2.3, and 2.5 nm, respectively, as shown in Figure 6a. In any case, the interparticle spacing is shorter by ~1 nm than the sum of two ligand lengths (Figure 6a, solid line). These shorter interparticle spacings are quite reasonable when one considers the interligand overlap between the neighboring BIP groups (ca. 0.8 nm), as illustrated in Figure 6b. The MM2 calculation of the TC_8BIP ligand revealed that the two benz-

(45) Heath, J. R.; Knobler, C. M.; Leff, D. V. *J. Phys. Chem. B* **1997**, *101*, 189−197.

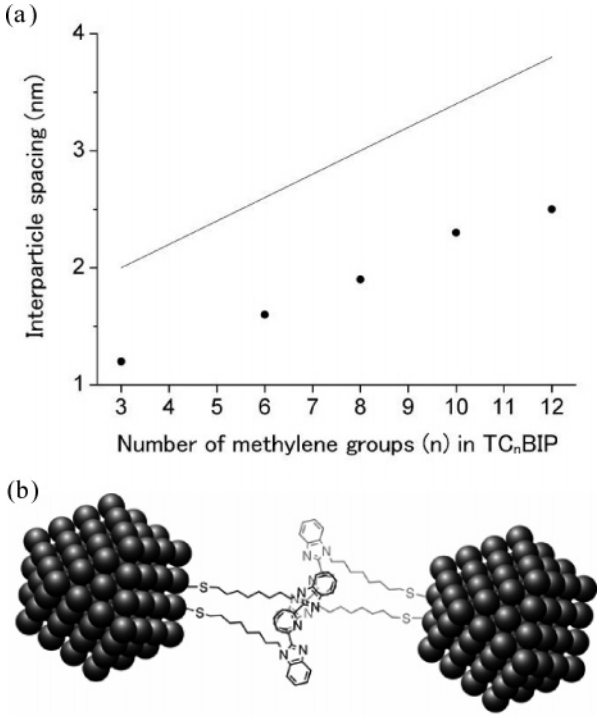

Figure 6. (a) Relationship between the interparticle spacings of 2D monolayers and the ligand lengths. The solid line stands for the length of two TC_nBIP ligands calculated on the assumption that the alkyl chains of TC_nBIP ligands have an all-trans conformation. (b) Schematic illustration of the interligand $\pi-\pi$ interaction between the neighboring TC_8BIP-Au nanoparticles.

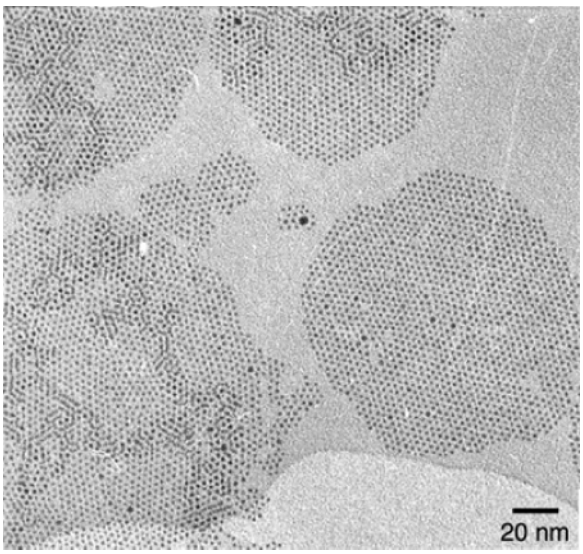

Figure 7. TEM image of self-assembled hcp domains of 1.5 nm TC_8BIP-Au nanoparticles formed at the air−water interface.

imidazole groups of the TC_8BIP ligand were distorted to the same direction, and the distortion angle between the benzimidazole and pyridine rings was smaller than 20°, indicating that the $\pi-\pi$ interaction between the neighboring highly crystalline BIP groups may stabilize the hcp superlattice.

The formation of hcp superlattices of TC_8BIP-Au nanoparticles is clearly observed at the air−water interface, where the particles easily combine to form a stable superstructure, as compared with the solid carbon surface. When a few microliters of a 5 mM chloroform solution of 1.5 nm TC_8BIP-Au nanoparticles was spread on water, the nanoparticles self-

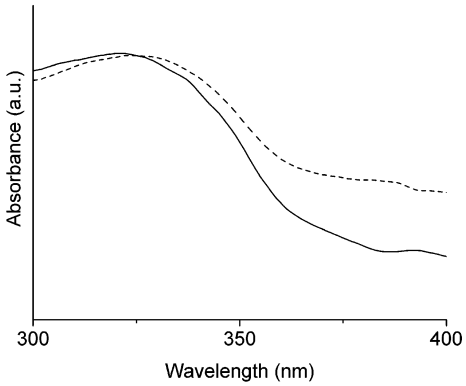

Figure 8. UV−vis spectra of TC_8BIP−Au nanoparticles on quartz substrates. TC_8BIP−Au nanoparticle chloroform solutions of (a) 3 mM (dotted line) and (b) 30 mM (solid line) concentration were deposited. The spectra were normalized with BIP $\pi-\pi^*$ absorbance.

assembled into a number of isolated hcp domains (∼100 nm × ∼100 nm, Figure 7). The mean interparticle spacing between the neighboring particle edges is estimated from the TEM image to be 1.9 ± 0.3 nm, which is compatible with that for the self-assembled superlattices directly formed on an amorphous-carbon-coated copper grid, indicating that the interligand $\pi-\pi$ interaction also induces the formation of hcp superlattices at the air−water interface. The interligand $\pi-\pi$ interaction was also implied by the small-angle X-ray diffraction of 1.5 nm TC_8-BIP−Au nanoparticle powder (Figure S1 in the Supporting Information), which was obtained by the precipitation from a TC_8BIP−Au DMF solution with methanol. The mean interparticle spacing was calculated as 2.2 nm from a diffraction peak at 2.06° assigned to the (111) plane for the 3D superlattice of 1.5 nm TC_8BIP−Au nanoparticles. This value is roughly consistent with that for a 2D superlattice within error, indicating that there is an interdigitation or overlap of BIP groups (0.8 nm).

The UV−vis spectra of different amounts of TC_8BIP−Au nanoparticles on quartz substrates were measured to spectroscopically confirm the existence of a $\pi-\pi$ interaction (Figure 8). TC_8BIP−Au nanoparticle chloroform solutions with two concentrations (3 and 30 mM) were deposited onto quartz substrates to form self-assembled domains of nanoparticles. The absorption peak of the BIP groups for 3 mM TC_8BIP−Au nanoparticles was centered at 324 nm, whereas that of the 30 mM nanoparticles occurs at 321 nm. Since highly concentrated nanoparticles form multilayer topology, the extent of $\pi-\pi$ stacking between the BIP rings is much higher in the vertical

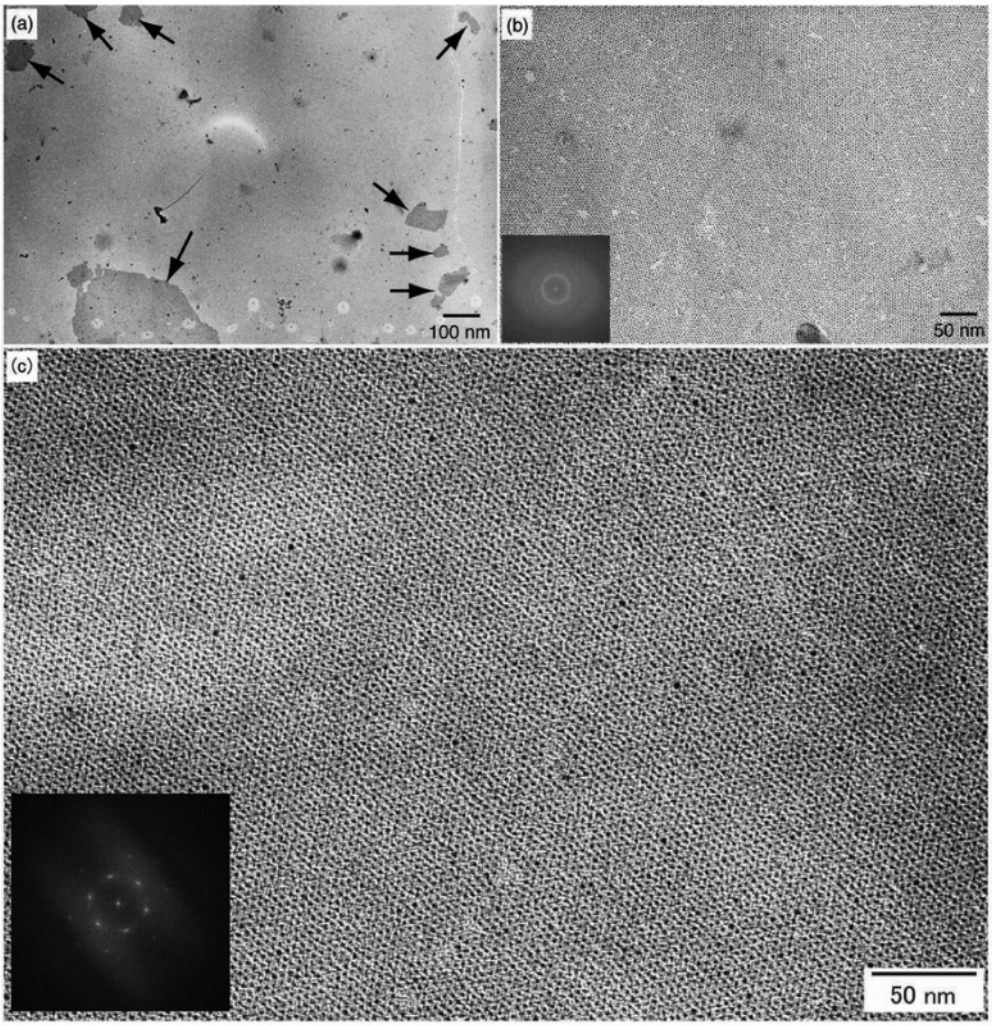

Figure 9. (a) Low-magnification TEM image of long-range-ordered hcp 2D superlattices of 1.5 nm TC_8BIP−Au nanoparticles after annealing at 50 °C for 12 h. The dark domains indicated by arrows are bilayers. (b) Enlarged TEM image of (a). (c) TEM image of a nearly perfectly ordered hcp 2D superlattice of 1.5 nm TC_8BIP−Au nanoparticles. The insets show FFT spots of each superlattice.

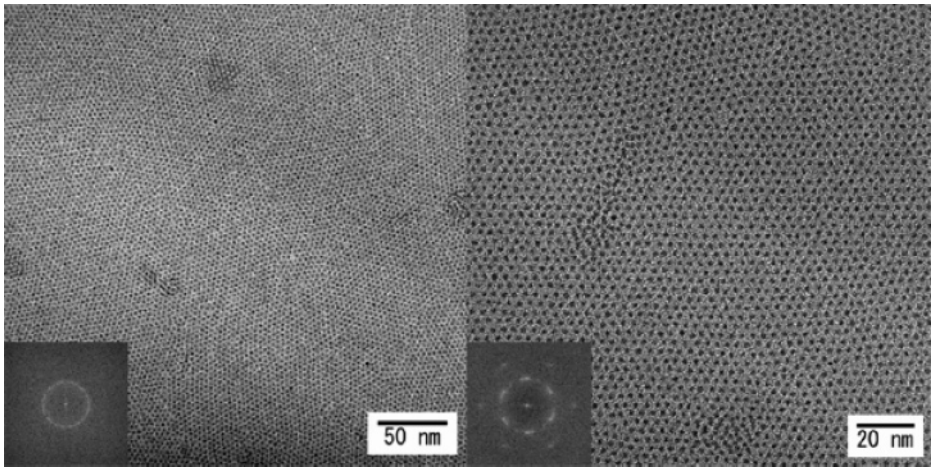

Figure 10. TEM images of long-range-ordered hcp 2D superlattices of 1.6 nm $TC_6BIP-Au$ nanoparticles after annealing at 50 °C for 12 h. The insets show FFT spots of each superlattice.

direction to the substrate. This 3 nm blue shift of the absorption peak clearly demonstrates the interligand $\pi-\pi$ interactions. A similar blue shift of the Soret band is observed for the porphyrin H-aggregate, in which porphyrin molecules are in a face-to-face π-stacking fashion.[46] Consequently, we concluded that the face-to-face interligand $\pi-\pi$ stacking shown in Figure 6b is responsible for the self-assembly of small $TC_nBIP-Au$ nanoparticles, and the interparticle spacing can be tuned by the ligand length even for small nanoparticle superlattices without any mechanical compression.

Heat-Induced Long-Range Ordering of $TC_8BIP-Au$ Nanoparticles at the Air−Water Interface. The long-range ordering of small nanoparticles is indispensable for measurement of the electron-transport property of nanoparticle superlattices. The Langmuir−Blodgett technique was first adopted for the formation of long-range-ordered 2D superlattices of $TC_8BIP-Au$ nanoparticles. The monodisperse 1.5 nm $TC_8BIP-Au$ nanoparticles were employed as these are small and easily self-assemble into hcp superlattices. In the surface pressure−occupied area ($\pi-A$) curve (Figure S2 in the Supporting Information), the surface pressure showed a gradual increase, although no sharp phase transition was observed. Due to the relatively strong interparticle interaction between the $TC_8BIP-Au$ nanoparticles, and in contrast to alkanethiol-protected Au nanoparticles, long-range-ordered superlattices were hardly obtained, and the resulting LB film consisted of a mixture of monolayer and multilayer domains with several vacant areas. It appears that the stiff small hcp domains of $TC_8BIP-Au$ nanoparticles remain unchanged even at high surface pressures, and these eventually overlap to form multilayer domains (Figure S3 in the Supporting Information). To convert the stiff hcp domains of $TC_8BIP-Au$ nanoparticles into a long-range-ordered hcp monolayer, it would be necessary to both weaken the interligand interaction and rearrange the nanoparticles. Our strategy was conceived from previous research on the thermal stability of LB monolayers of alkanethiol-protected Au and Ag nanoparticles reported by Heath and co-workers.[21,45] A solution (10 μL) of 1.5 nm $TC_8BIP-Au$ nanoparticles in chloroform (0.5 mM as Au atoms) was spread onto the water (18.2 MΩ cm^{-1}) phase in a 100 mL beaker, where the air−water interface area was 15 cm^2. Considering the total diameter of a single $TC_8BIP-Au$ nanoparticle (3.4 nm) and the fcc packing fashion, the total area of $TC_8BIP-Au$ nanoparticles on the water subphase is ca. 4 cm^2, which is small enough to both obtain a monolayer hcp 2D superlattice and avoid an unfavorable interaction between the glass wall and the nanoparticles. To avoid water evaporation, either the humidity inside the oven was adjusted to 100% or the beaker was covered with a polyethylene film. Then, the beaker was placed inside a sealed oven and annealed at 50 °C for 12 h to weaken the $\pi-\pi$ interaction between the TC_8BIP ligands and rearrange the Au nanoparticles. The obtained film was transferred onto an amorphous-carbon-coated copper grid by means of a horizontal lifting method. Figure 9 shows the TEM images of the film produced at the air−water interface after an annealing process. It was found from Figure 9a that this film predominantly consisted of a $TC_8BIP-Au$ nanoparticle monolayer with minor fragments of a bilayer (indicated by arrows in Figure 9a; the other dark spots mainly come from aerial dust). The enlarged image of the monolayer in Figure 9b demonstrates that the long-range-ordered hcp monolayer of 1.5 nm $TC_8BIP-Au$ nanoparticles was generated without large vacancies. It should be noted that such long-range-ordered superlattices were never observed before annealing. Fast Fourier transform (FFT) spots in the enlarged TEM image (see the inset in Figure 9b) are seen with a spacing corresponding to an interparticle spacing of the superlattice. With respect to the periodicity of the nanoparticles, the as-formed monolayer is not uniform, but rather an aggregate of many hcp domains, which is also suggested by the slight expanse of the FFT spots. Nearly perfect ordering was often observed (Figure 9c), and FFT spots proved the quite high ordering degree (see the inset in Figure 9c). The multicrystalline topology (Figure 9b) seems to be half the crystalline rearrangement formed during the annealing process. This interligand-interaction-based self-assembly process at the air−water interface is fundamentally different from previous methods, such as those relying on surface tension applied during annealing at room temperature,[47] self-assembly at the water/oil interface,[48,49]

(46) Imahori, H.; Norieda, H.; Nishimura, Y.; Yamazaki, I.; Higuchi, K.; Kato, N.; Motohiro, T.; Yamada, H.; Tamaki, K.; Arimura, M.; Sakata, Y. *J. Phys. Chem. B* **2000**, *104*, 1253−1260.

(47) Brown, J. J.; Porter, J. A.; Daghlian, C. P.; Gibson, U. J. *Langmuir* **2001**, *17*, 7966−7969.

(48) Lin, Y.; Skaff, H.; Emrick, T.; Dinsmore, A. D.; Russell, T. P. *Science* **2003**, *299*, 226−229.

or solvent evaporation rate controlled self-assembly,[50,51] because no liquid/liquid interface, surface tension, or other additives known to change the contact angle at the subphase have been used in our approach. Our approach exploits only the affinity between the aromatic groups of TC_nBIP ligands, which is similar to the crystalline growth process. To further extend this approach, 1.6 nm TC_6BIP−Au nanoparticles were also employed. After annealing at 50 °C for 12 h, an ordered hcp 2D superlattice was obtained (Figure 10), indicating that annealing-assisted self-assembly at the air−water interface can be applied to other nanoparticles capped by ligands with terminal highly crystalline groups. For the generation of perfectly ordered hcp superlattices, optimum temperatures and heating times should be applied, and further investigation is in progress.

Conclusions

We synthesized a series of TC_nBIP ligands (n = 3, 6, 8, 10, 12) bearing terminal π-conjugated bis(benzimidazol-2-yl)-pyridine groups and disulfides (or mercapto groups) at both ends. Small and monodisperse TC_nBIP−Au nanoparticles were successfully synthesized, and well-ordered hcp 2D superlattices were formed on amorphous-carbon membranes. Several small domains of well-ordered hcp 2D superlattices of TC_8BIP−Au nanoparticles were also formed at the air−water interface, and through an annealing process, these domains were converted into long-range-ordered superlattices through a rearrangement of the nanoparticles. The heat-induced rearrangement of the metal nanoparticle superlattice is potentially applied to other nanoparticles possessing relatively strong interparticle interactions. To the best of our knowledge, the self-assembly of stable, small nanoparticles into long-range well-ordered hcp superlattices has been accomplished only by using TC_nBIP−Au nanoparticles. The monolayer produced at the air−water interface can be advantageously transferred onto any substrate. The interparticle spacings of TC_nBIP−Au nanoparticles are simply controlled by changing the ligand length from 1.2 nm for TC_3BIP−Au to 2.5 nm for TC_{12}BIP−Au nanoparticles. Especially, the spacing of 1.2 nm for TC_3BIP−Au nanoparticles is narrow enough to realize interparticle electron tunneling, and easy handling, due to their excellent stability, may open new doors to producing high-quality single-electron-tunneling devices. Investigations into the electron-transport property of the hcp superlattice of TC_nBIP−Au nanoparticles using double-probe STM or nanogap gold electrodes is currently in progress and is expected to reveal the effect of π-conjugated terminal aromatic groups.

Experimental Section

Materials. All chemicals were purchased from Sigma-Aldrich, Wako Chemical, Kanto Chemical, and Tokyo Kasei Kogyo and used as is without further purification unless otherwise noted.

Ligand Syntheses. 10-Bromo-1-decene (1). To a solution of 9-decen-1-ol (2.42 g, 15.5 mmol) in dry THF (50 mL) were added triphenylphosphine (4.09 g, 15.6 mmol) and tetrabromomethane (5.10 g, 15.5 mmol) under cooling with a water bath at room temperature, and the solution was stirred for 2.5 h. The resulting triphenylphosphine oxide was filtered off, and the filtrate was concentrated under reduced pressure. The product was purified by column chromatography (silica gel, hexane) to give **1** (3.40 g, equivalent yield) as a colorless oil. ^{1}H NMR (400 MHz, $CDCl_3$): δ 1.85 (q, 6H), 2.04 (q, 2H), 3.40 (t, 2H), 4.96 (m, 2H), 5.81 (m, 1H). GC−MS (EI): *m*/*z* 218, calcd exact mass 218.067.

2,6-Bis(1′-(prop-2-enyl)benzimidazol-2-yl)pyridine (2a). Sodium hydride (NaH, 60%) in oil (644 mg, 16.1 mmol) was added to a three-necked flask under an argon atmosphere, and then dry hexane was added. After the resulting solution was stirred for 5 min, the hexane was removed with a syringe, and dry *N*,*N*-dimethylacetamide (DMAc; 30 mL) was then added. BIP **(**1.00 g, 3.20 mmol) was added and the mixture heated to 50 °C for 2 h. To this solution was added 3-bromo-1-propene (7.16 mL, 82.8 mmol), and the mixture was continuously heated for 2 h. The solution was then cooled to room temperature, and dichloromethane was added. The resulting pale yellow solution was washed with water, dried over Na_2SO_4, and concentrated under reduced pressure. The product was purified by column chromatography (silica gel, ethyl acetate:methanol = 99:1) to give **2a** (2.60 g, equivalent yield) as a colorless powder. ^{1}H NMR (300 MHz, $CDCl_3$): δ 4.70 (t, 4H), 4.84 (t, 1H), 5.12 (t, 1H), 5.41 (m, 4H), 7.37 (m, 4H), 7.48 (m, 2H), 7.91 (q, 2H), 8.03 (t, 1H), 8.38 (d, 2H). DI-MS (EI): *m*/*z* 391, calcd exact mass 391.18.

2,6-Bis(1′-(hex-5-enyl)benzimidazol-2-yl)pyridine (2b). NaH (60%) in oil (1.28 g, 32.1 mmol) was added to a three-necked flask under an argon atmosphere, and then dry hexane was added. After the resulting solution was stirred for 5 min, the hexane was removed with a syringe, and dry DMAc (30 mL) was then added. BIP (2.00 g, 6.40 mmol) was added, and the mixture was heated to 80 °C for 2 h. To this solution was added 6-bromo-1-hexene (2.27 mL, 16.9 mmol), and the mixture was continuously heated for 2 h. The solution was then cooled to room temperature, and dichloromethane was added. The resulting pale yellow solution was washed with water, dried over Na_2SO_4, and concentrated under reduced pressure. The product was purified by column chromatography (silica gel, ethyl acetate:methanol = 99:1) to give **2b** (3.05 g, equivalent yield). ^{1}H NMR (300 MHz, $CDCl_3$): δ 1.21 (m, 8H), 1.83 (m, 8H), 4.78 (m, 8H), 7.37 (m, 4H), 7.48 (m, 2H), 7.86 (m, 2H), 8.07 (t, 1H), 8.33 (d, 2H). DI-MS (EI): *m*/*z* 475, calcd exact mass 475.27.

2,6-Bis(1′-(oct-7-enyl)benzimidazol-2-yl)pyridine (2c). NaH (60%) in oil (552 mg, 13.8 mmol) was added to a three-necked flask under an argon atmosphere, and then dry hexane was added. After the resulting solution was stirred for 5 min, the hexane was removed with a syringe, and dry DMAc (30 mL) was then added. BIP (1.79 g, 5.75 mmol) was added and the resulting solution stirred at 80 °C for 2 h. To this solution was added 8-bromo-1-octene (3.47 mL, 20.7 mmol), and the resulting mixture was continuously heated at 80 °C for 2 h. The solution was then cooled to room temperature, and diethyl ether was added. The resulting pale yellow solution was washed with water, dried over Na_2SO_4, and concentrated under reduced pressure. The product was purified by column chromatography (silica gel, hexane:ethyl acetate:methanol = 4:1:1) to give **2c** (3.25 g, equivalent yield). ^{1}H NMR (300 MHz, $CDCl_3$): δ 1.08 (m, 12H), 1.76 (m, 8H), 4.70 (t, 4H), 4.84 (m, 4H), 5.62 (m, 2H), 7.37 (m, 4H), 7.47 (m, 2H), 7.88 (m, 2H), 8.06 (t, 1H), 8.32 (d, 2H). DI-MS (EI): *m*/*z* 531, calcd exact mass 531.336.

2,6-Bis(1′-(dec-9-enyl)benzimidazol-2-yl)pyridine (2d). NaH (60%) in oil (432 mg, 10.8 mmol) was added to a three-necked flask under an argon atmosphere, and then dry hexane was added. After the resulting solution was stirred for 5 min, the hexane was removed with a syringe, and dry DMAc (30 mL) was then added. BIP (1.12 g, 3.60 mmol) was added, and the mixture was heated to 80 °C for 1 h. To this solution was added **1** (2.37 g, 10.8 mmol), and the mixture was continuously stirred at 70 °C for 17 h. The solution was then cooled to room temperature, and diethyl ether was added. The resulting pale yellow solution was washed with water, dried over Na_2SO_4, and concentrated under reduced pressure. The product was purified by column chroma-

(49) Reincke, F.; Hickey, S. G.; Kegel, W. K.; Vanmaekelbergh, D. *Angew. Chem., Int. Ed.* **2004**, *43*, 458−462.
(50) Lin, X. M.; Jaeger, H. M.; Sorensen, C. M.; Klabunde, K. J. *J. Phys. Chem. B* **2001**, *105*, 3353−3357.
(51) Narayanan, S.; Wang, J.; Lin, X.-M. *Phys. Rev. Lett.* **2004**, *93*, 135503-(1−4).

tography (silica gel, hexane:ethyl acetate = 1:1) to give **2d** (1.73 g, 82%). ^{1}H NMR (300 MHz, $CDCl_3$): δ 1.08 (m, 12H), 1.76 (m, 8H), 4.70 (t, 4H), 4.84 (m, 4H), 5.62 (m, 2H), 7.35 (m, 4H), 7.45 (m, 2H), 7.87 (m, 2H), 8.05 (t, 1H), 8.31 (d, 2H). DI-MS (EI): *m*/*z* 587, calcd exact mass 587.399.

2,6-Bis(1′-(12-bromododecyl)benzimidazol-2-yl)pyridine (2e). NaH (60%) in oil (770 mg, 19.3 mmol) was added to a three-necked flask under an argon atmosphere, and then dry hexane was added. After the resulting solution was stirred for 5 min, the hexane was removed with a syringe, and dry DMAc (10 mL) was then added. BIP (2.0 g, 6.4 mmol) was added, and the resulting mixture was heated to 75 °C for 1 h. This pale yellow solution was added to the preheated dry DMAc solution (10 mL) of 1,12-dibromododecane (3.35 mL, 28.3 mmol) through a needle at 75 °C, and the mixture was continuously heated for 1 h. The solution was then cooled to room temperature, and diethyl ether was added. The resulting pale yellow solution was washed with water, dried over Na_2SO_4, and concentrated under reduced pressure. The product was purified by column chromatography (silica gel, hexane, then ethyl acetate:methanol = 100:1) to give **2e** (3.88 g, 75%). ^{1}H NMR (300 MHz, $CDCl_3$): δ 1.08 (m, 12H), 1.76 (m, 8H), 4.70 (t, 4H), 4.84 (m, 4H), 5.62 (m, 2H), 7.35 (m, 4H), 7.45 (m, 2H), 7.87 (m, 2H), 8.05 (t, 1H), 8.31 (d, 2H). DI-MS (EI): *m*/*z* 805, calcd exact mass 805.312

2,6-Bis(1′-(3-thioacetoxylpropyl)benzimidazol-2-yl)pyridine (3a). A dichloromethane solution (50 mL) of **2a** (1.26 g, 320 mmol) and thioacetic acid (0.69 mL, 9.7 mmol) was irradiated with a high-pressure mercury lamp (400 W) under argon for 2 h. The solution was washed with saturated aqueous $NaHCO_3$ solution, dried over Na_2SO_4, and concentrated under reduced pressure. The product was purified by column chromatography (silica gel, dichloromethane:ethyl acetate = 3:1) to give **3a** (1.31 g, 75%) as a pale yellow oil. ^{1}H NMR (300 MHz, $CDCl_3$): δ 1.97 (s, 4H), 2.03 (m, 4H), 2.70 (t, 4H), 4.76 (t, 4H), 7.37 (m, 4H), 7.48 (m, 2H), 7.91 (q, 2H), 8.03 (t, 1H), 8.38 (d, 2H). DI-MS (EI): *m*/*z* 543, calcd exact mass 543.18.

2,6-Bis(1′-(6-thioacetoxyhexyl)benzimidazol-2-yl)pyridine (3b). A dichloromethane solution (50 mL) of **2b** (3.05 g, 6.40 mmol) and thioacetic acid (1.37 mL, 19.2 mmol) was irradiated with a high-pressure mercury lamp (400 W) under argon for 2 h. The solution was washed with saturated aqueous $NaHCO_3$ solution, dried over Na_2SO_4, and concentrated under reduced pressure. The product was purified by column chromatography (silica gel, dichloromethane:ethyl acetate = 3:1) to give **3b** (4.02 g, equivalent yield) as a pale yellow oil. ^{1}H NMR (300 MHz, $CDCl_3$): δ 1.10 (m, 8H), 1.27 (m, 4H), 1.86 (m, 4H), 2.20 (s, 6H), 2.61 (t, 4H), 4.69 (t, 4H), 7.33 (m, 4H), 7.45 (m, 2H), 7.86 (m, 2H), 8.06 (t, 1H), 8.32 (d, 2H). DI-MS (EI): *m*/*z* 627, calcd exact mass 627.27.

2,6-Bis(1′-(8-thioacetoxyoctyl)benzimidazol-2-yl)pyridine (3c). A dichloromethane solution (50 mL) of **2c** (2.41 g, 4.53 mmol) and thioacetic acid (3.2 mL, 45.3 mmol) was irradiated with a high-pressure mercury lamp (400 W) under argon for 3 h. The solution was washed with saturated aqueous $NaHCO_3$ solution, dried over Na_2SO_4, and concentrated under reduced pressure. The product was purified by column chromatography (silica gel, hexane:dichloromethane:methanol = 5:5:1) to give **3c** (3.09 g, equivalent yield) as a pale yellow oil. ^{1}H NMR (300 MHz, $CDCl_3$): δ 1.02−1.25 (m, 16H), 1.33 (m, 4H), 1.75 (m, 4H), 2.30 (s, 6H), 2.71 (t, 4H), 4.69 (t, 4H), 7.36 (m, 4H), 7.47 (m, 2H), 7.87 (m, 2H), 8.07 (t, 1H), 8.31 (d, 2H). DI-MS (EI): *m*/*z* 683, calcd exact mass 683.333.

2,6-Bis(1′-(10-thioacetoxydecyl)benzimidazol-2-yl)pyridine (3d). A dichloromethane solution (50 mL) of **2d** (1.68 g, 2.86 mmol) and thioacetic acid (2.0 mL, 28.6 mmol) was irradiated with a high-pressure mercury lamp (400 W) under argon for 3 h. The solution was washed with saturated aqueous $NaHCO_3$ solution, dried over Na_2SO_4, and concentrated under reduced pressure. The product was purified by column chromatography (silica gel, hexane:ethyl acetate = 1:1) to give **3d** (2.09 g, 99%) as a pale yellow oil. ^{1}H NMR (300 MHz, $CDCl_3$): δ 1.00−1.25 (m, 24H), 1.50 (m, 4H), 1.73 (m, 4H), 2.31 (s, 6H), 2.84 (t, 4H), 4.71 (t, 4H), 7.36 (m, 4H), 7.47 (m, 2H), 7.87 (m, 2H), 8.06 (t, 1H), 8.32 (d, 2H). DI-MS (EI): *m*/*z* 739, calcd exact mass 739.395.

2,6-Bis(1′-(12-thioacetoxydodecyl)benzimidazol-2-yl)pyridine (3e). An acetonitrile solution (100 mL) of **2e** (3.57 g, 4.4 mmol) was bubbled with Ar for 5 min. To this solution was added potassium thioacetate (1.26 g, 11.1 mmol), and the resulting mixture was stirred under argon at room temperature for 2 h. The solvent was removed under reduced pressure, diethyl ether was added, and the solution was washed with saturated aqueous $NaHCO_3$ solution, dried over Na_2SO_4, and concentrated under reduced pressure. The product was purified by column chromatography (silica gel, dichloromethane:ethyl acetate = 3:1) to give **3e** (3.56 g, equivalent yield) as a pale yellow oil. ^{1}H NMR (300 MHz, $CDCl_3$): δ 1.00−1.25 (m, 32H), 1.54 (m, 4H), 1.71 (m, 4H), 2.32 (s, 6H), 2.85 (t, 4H), 4.71 (t, 4H), 7.33 (m, 4H), 7.45 (m, 2H), 7.87 (m, 2H), 8.06 (t, 1H), 8.32 (d, 2H). DI-MS (EI): *m*/*z* 795, calcd exact mass 795.458.

2,6-Bis(1′-(3-mercaptopropyl)benzimidazol-2-yl)pyridine (4a). Sodium borohydride (1.31 g, 2.4 mmol) was added to a DMAc solution (50 mL) of **3a** (1.31 g, 2.4 mmol). The mixture was stirred at room temperature for 1 h. After addition of water to the solution, the product was extracted with dichloromethane, dried over Na_2SO_4, and concentrated under reduced pressure. The product was then purified by column chromatography (silica gel, dichloromethane:ethyl acetate = 3:1) to give **4a** (0.5 g, 93%) as a colorless solid. ^{1}H NMR (300 MHz, $CDCl_3$): δ 2.32 (m, 4H), 2.94 (q, 4H), 4.79 (t, 4H), 7.33 (m, 4H), 7.45 (m, 2H), 7.86 (q, 2H), 8.06 (t, 1H), 8.31 (d, 2H). DI-MS (EI): *m*/*z* 459, calcd exact mass 459.16.

2,6-Bis(1′-(6-thiohexyl)benzimidazol-2-yl)pyridine (4b). Sodium methoxide (2.04 g, 38 mmol) was added to a 2-propanol solution (500 mL) of **3b** (1.00 g, 1.6 mmol), and the mixture was vigorously stirred under ambient conditions at room temperature for 48 h. The solvent was removed under reduced pressure. After addition of water to the solution, the product was extracted with chloroform, dried over Na_2SO_4, and concentrated under reduced pressure. The product was then purified by column chromatography (silica gel, dichloromethane:ethyl acetate = 3:1) to give **4b** (0.77 g, 89%) as a colorless solid. ^{1}H NMR (300 MHz, $CDCl_3$): δ 1.11 (m, 8H), 1.76 (m, 4H), 4.70 (t, 4H), 4.85 (t, 4H), 7.35 (m, 4H), 7.46 (m, 2H), 7.88 (m, 2H), 8.07 (t, 1H), 8.32 (d, 2H). DI-MS (EI): *m*/*z* 541, calcd exact mass 541.23.

2,6-Bis(1′-(8-thiooctyl)benzimidazol-2-yl)pyridine (4c). Sodium methoxide (2.04 g, 38 mmol) was added to a 2-propanol solution (500 mL) of **3c** (1.02 g, 1.5 mmol), and the mixture was vigorously stirred under ambient conditions at room temperature for 48 h. The solvent was removed under reduced pressure. After addition of water to the solution, the product was extracted with chloroform, dried over Na_2SO_4, and concentrated under reduced pressure. The product was then purified by column chromatography (activated alumina, chloroform) to give **4c** (0.83 g, 93%) as a colorless solid. ^{1}H NMR (300 MHz, $CDCl_3$): δ 1.28 (m, 16H), 1.65 (m, 4H), 1.84 (m, 4H), 2.66 (t, 4H), 4.73 (t, 4H), 7.36 (m, 4H), 7.48 (m, 2H), 7.87 (m, 2H), 8.05 (t, 1H), 8.34 (d, 2H). ESI-FT-ICR-MS: *m*/*z* 598.303 ($M + H^+$), calcd exact mass 598.304 (M + H).

2,6-Bis(1′-(10-thiodecyl)benzimidazol-2-yl)pyridine (4d). An aqueous solution (5 mL) of potassium carbonate (0.30 g, 2.2 mmol) was added to an ethanol solution (300 mL) of **3d** (0.35 g, 0.47 mmol). The mixture was vigorously stirred under ambient conditions at room temperature for 48 h. The solvent was removed under reduced pressure. After addition of water to the solution, the product was extracted with chloroform, dried over Na_2SO_4, and concentrated under reduced pressure. The product was then purified by column chromatography (activated alumina, chloroform) to give **4d** (0.25 g, 80%) as a colorless solid. ^{1}H NMR (300 MHz, $CDCl_3$): δ 1.23 (m, 20H), 1.37 (m, 4H), 1.68 (m, 4H), 1.83 (m, 4H), 2.69 (t, 4H), 4.71 (t, 4H), 7.38 (m, 4H), 7.47 (m, 2H), 7.88 (m, 2H), 8.05 (t, 1H), 8.34 (d, 2H). ESI-FT-ICR-MS: *m*/*z* 654.366 ($M + H^+$), calcd exact mass 654.366 (M + H).

2,6-Bis(1′-(12-thiododecyl)benzimidazol-2-yl)pyridine (4e). Sodium methoxide (1.02 g, 18.8 mmol) was added to a 2-propanol solution (500 mL) of **3e** (0.50 g, 0.63 mmol). The mixture was vigorously stirred under ambient conditions at room temperature for 72 h. The solvent was removed under reduced pressure. After addition of water to the solution, the product was extracted with chloroform, dried over Na_2SO_4, and concentrated under reduced pressure. The product was then purified by column chromatography (activated alumina, chloroform) to give **4e** (0.32 g, 71%) as a colorless solid. ^{1}H NMR (300 MHz, $CDCl_3$): δ 1.13−1.40 (m, 32H), 1.67 (m, 4H), 1.82 (m, 4H), 2.70 (t, 4H), 4.69 (t, 4H), 7.37 (m, 4H), 7.48 (m, 2H), 7.89 (m, 2H), 8.07 (t, 1H), 8.33 (d, 2H). ESI-FT-ICR-MS: m/z 710.428 (M + H$^+$), calcd exact mass 710.429 (M + H).

Preparation of TC_nBIP−Au Nanoparticles. In a typical preparation, 2.5 mL of a 1 mM aqueous solution of $HAuCl_4 \cdot 4H_2O$ (2.5 μmol) was added to a mixture of 1 mL of a 2.5 mM DMF solution of TC_nBIP (2.5 μmol) and 44 mL of DMF. After the solution was heated at 60 °C or cooled in an ice−water bath, 2.5 mL of a 10 mM aqueous solution of $NaBH_4$ (25 μmol) was swiftly added to the solution under vigorous stirring, and the solution was continuously stirred for 1 h to obtain TC_nBIP−Au nanoparticles. The solvent was evaporated to ca. 3 mL at 40 °C under reduced pressure. Distilled methanol was then added, and the mixture was centrifuged to give a crude precipitate of Au nanoparticles. The precipitate was dissolved in 0.5 mL of distilled chloroform, reprecipitated with distilled methanol, and centrifuged. The reprecipitation processes were repeated three times to give pure TC_nBIP-protected Au nanoparticles.

Measurements. The consumption of $AuCl_4^-$ ions and the formation of TC_nBIP−Au nanoparticles were confirmed by UV−vis spectroscopy with a Hitachi U-3310 UV−vis spectrophotometer. The ligand contents of TC_nBIP−Au nanoparticles were estimated by TGA on an ULVAC-RIKO TGD9700 by heating from room temperature to 600 °C at a heating rate of 2 °C min^{-1} and holding at 600 °C for 30 min. FT-IR spectroscopy (HORIBA FT-720) was adopted to investigate the conformation of the TC_nBIP ligands on Au nanoparticles in the solid state by a KBr method. The Au nanoparticles were observed by TEM at 100 kV on a Hitachi H-7100. The crystal structure of the Au nanoparticles was determined by both HRTEM at 300 kV on a Hitachi H-9000NAR and XRD on a MAC Science M18XHF-SRA with Cu Kα radiation. XPS was used to examine the chemical state of the sulfur in the TC_nBIP nanoparticles and gold core. The S2p and Au4f peaks of the TC_nBIP−Au nanoparticles were measured on an Ulvac Phi 5600ci with monochromated Al X-ray radiation at 350 W.

Particle Size and Interparticle Spacing Distribution Measurements. Particle size distributions were measured by counting 200 of nanoparticles for each TC_nBIP−Au monolayer on an amorphous-carbon-coated copper grid. The mean interparticle spacing was obtained by direct measurement of the individual spacings in a well-ordered hcp domain.

Acknowledgment. The present work was supported by the Industrial Technology Research Grant Program in ’04 from NEDO of Japan, a Grant-in-Aid for Scientific Research on Priority Area “Chemistry of Coordination Space” from MEXT (T.T.), and a Grant-in-Aid for Young Scientists (B) (No. 17710090) from MEXT, Japan (M.K.).

Supporting Information Available: Small-angle X-ray diffraction pattern of 1.5 nm TC_8BIP−Au nanoparticle powder, $\pi-A$ curve of a TC_8BIP−Au nanoparticle LB film, and TEM image of a 1.5 nm TC_8BIP−Au nanoparticle LB film obtained at 15 mN/m. This material is available free of charge via the Internet at http://pubs.acs.org.

JA064510Q